

2 (Mis)Identification of magmatic and exhumation ages by
3 detrital zircon U-Pb and He double dating: a case study
4 from the Bergell-Gonfolite system (European Alps)

5 Marco G. Malusà ^{1*}, Owen A. Anfinson ², Daniel F. Stockli ³

6 ¹ Department of Earth and Environmental Sciences, University of Milano-Bicocca, Piazza della
7 Scienza 4, 20126 Milan, Italy

8 ² Department of Geology, Sonoma State University, 1801 East Cotati Avenue, Rohnert Park,
9 Rohnert Park, California 94928, USA

10 ³ Department of Geological Sciences, Jackson School of Geosciences, University of Texas at
11 Austin, 1 University Station C1100, Austin, Texas 78712, USA

12 *Corresponding author at: Department of Earth and Environmental Sciences, University of Milano-Bicocca, Piazza
13 della Scienza 4, 20126 Milan, Italy. E-mail address: marco.malusa@unimib.it (M.G. Malusà)

14 **Abstract**

15 Reliable interpretation of detrital thermochronometric datasets requires correct attribution of
16 these ages as either the record of exhumational cooling or the record of post-magmatic cooling
17 independent of tectonic or erosional exhumation. A classic approach for identifying magmatic cooling
18 ages is through double dating leveraging paired high- and low-temperature geo/thermochronologic
19 systems, which should yield, within error, indistinguishable ages from the same grain. On the
20 contrary, low-temperature thermochronometric ages that are younger than their corresponding
21 crystallization ages are mostly invariably interpreted to record exhumation. Here, we test this last
22 assumption by applying a detrital zircon U-Pb and (U-Th)/He double-dating approach to a well-
23 constrained source-to-sink system in the southern European Alps, archiving the progressive unroofing
24 of the Bergell-Novate volcanic-plutonic complex and associated country rocks. We depth-profile U-

25 Pb dated unpolished detrital zircon grains and performed (U-Th)/He analysis on non-
26 volcanic/plutonic grains. Of the double-dated grains, 40% yielded (U-Th)/He ages overlapped in age
27 with Bergell-Novate magmatism (32-30 and 27-24 Ma). Despite yielding (U-Th)/He ages younger
28 than their corresponding U-Pb ages, these ages record post-magmatic cooling within the contact
29 aureole and not exhumation. Our findings indicate that only a fraction of the grains yielding magmatic
30 He ages can be identified by double dating, and that the assumption that all the remaining grains
31 constrain exhumation can be potentially misleading. Finally, we present improved criteria for the
32 interpretation of detrital zircon thermochronometric double-dating results and conclude that many
33 previous interpretations based on a classic double-dating approach should be reconsidered in syn-
34 magmatic orogenic systems.

35 **Keywords:** Zircon double dating; detrital thermochronology; post-magmatic cooling; exhumation;
36 lag-time analysis; European Alps.

37 1. Introduction

38 Detrital thermochronometric analyses of apatite and zircon grains are increasingly employed to
39 develop quantitative models of deep-time landscape evolution and constrain rates of erosional
40 exhumation (e.g., [Govin et al. 2020](#); [Lang et al. 2020](#); [Lossada et al. 2020](#); [Stockli and Najman 2020](#)).
41 Many of these studies are based on the lag-time approach, which compares thermochronometric ages
42 recorded by mineral grains in sedimentary strata to the corresponding stratigraphic ages, which are
43 independently determined (e.g., [Garver et al. 1999](#); [Bernet et al. 2006](#)). However, a crucial assumption
44 for the validity of this application is the correct discrimination between thermochronometric ages,
45 recording cooling due to exhumation, i.e., the motion of parent rocks towards Earth's surface
46 ([England and Molnar 1990](#)) and thermochronometric ages that record cooling independent of
47 exhumation, such as post-magmatic cooling of volcanic and shallow-level plutonic rocks ([Malusà
48 and Fitzgerald 2019a](#)). A classic approach for the identification of magmatic crystallization ages in
49 detrital thermochronometric studies is by double dating, combining U-Pb and low-temperature

50 thermochronometric dating on the same mineral grain (Carter and Moss 1999; Reiners et al. 2005)
51 (Fig. 1). Magmatic zircon from volcanic or shallow-level plutonic rocks should display within error
52 indistinguishable U–Pb and fission-track or (U–Th)/He ages (ZUPb, ZFT and ZHe hereafter), due to
53 rapid post-crystallization cooling in the upper crust where country rocks are at temperatures below
54 closure isotherms or the partial annealing (or retention) zones of the ZFT or ZHe systems (Malusà et
55 al. 2011; Saylor et al. 2012). Zircon grains crystallized at high temperatures (i.e., greater depths)
56 record cooling during subsequent exhumation and hence should yield ZFT and ZHe ages younger
57 than their corresponding ZUPb ages and may reveal the long-term exhumation history of the source
58 terrane. These cooling ages can be leveraged in the lag-time approach, provided that a range of
59 fundamental assumptions are met and can be properly evaluated (Malusà and Fitzgerald 2020).

60 Implicit assumption of many detrital double-dating thermochronology studies is that all the grains
61 yielding magmatic ages can be readily identified by their ZUPb=ZFT or ZUPb=ZHe fingerprint (1 in
62 Fig. 1), and that all the remaining grains (2 and 3 in Fig. 1) provide meaningful constraints on the
63 exhumation history of the source terrane (e.g., Najman et al. 2010; Stevens et al. 2013; Jourdan et al.
64 2013, 2018; Bootes et al. 2019; Lu et al. 2020; Pujols and Stockli 2021). However, this may be an
65 inappropriate assumption in magmatic terranes or at least an oversimplification (Reiners et al. 2005).
66 In this study, we explore the possibility that a portion of the magmatic ages in detrital
67 thermochronometric dataset, for example those “magmatic ages” recording country-rock cooling
68 within a contact aureole, might be systematically overlooked by a double-dating approach with major
69 implications for lag-time interpretations in certain geologic settings. To explore this issue and its
70 implications, we apply ZUPb and ZHe double dating to detrital zircon grains of the Gonfolite Group,
71 an Oligocene-Miocene proximal foreland basin sedimentary succession largely derived from erosion
72 of the Bergell/Bregaglia volcanic-plutonic complex and associated country rocks (Wagner et al. 1979;
73 Bernoulli et al. 1993). The Bergell-Gonfolite system is an ideal field laboratory for our study because
74 its mineral-age stratigraphy, i.e., the specific combinations of crystallization and exhumation ages of

75 different thermochronometers at different depths in the crust, is extremely well constrained (Malusà
76 et al. 2011, 2016; Fitzgerald et al. 2019).

77 We dated with the ZHe method, zircons of the Gonfolite Group with Paleozoic U-Pb ages from
78 the zircon rim. In this way, we could be sure that the grains come from the country rock and not from
79 the Bergell pluton and associated magmatic rocks. As these zircons come from stratigraphic units in
80 which it is known from the literature that the AFT ages in country-rock cobbles are pre-intrusion, and
81 because the AFT system is a lower temperature chronometer than the ZHe system, the expectation
82 was to obtain pre-intrusion ZHe ages. Despite this, we found that 40% of the grains show ZHe ages
83 overlapping with the age of the intrusions. We interpret these ZHe ages as recording post-magmatic
84 cooling within the contact aureole of the plutons and not exhumation.

85 Based on our new results, we define improved criteria for correct identification of post-magmatic
86 and exhumational cooling ages in detrital thermochronometry studies. These criteria are illustrated
87 by applying them to high-quality published double-dating datasets from the literature. Our findings
88 suggest that the interpretation of many previously published detrital thermochronology datasets
89 should be carefully reevaluated and potentially reconsidered.

90 **2. Geologic and thermochronologic setting**

91 ***2.1. The Bergell-Gonfolite source-to-sink system***

92 The Bergell pluton is exposed in the Central Alps and was intruded at 32-30 Ma into Alpine
93 metamorphic rocks (von Blanckenburg 1992; Ji et al. 2019). It consists of a tonalitic–granodioritic
94 main body and a tail-shaped feeder zone parallel to the Insubric Fault (Fig. 2a). The contact aureole
95 of the pluton is largely eroded away and is exclusively preserved around its eastern part, where it is
96 1.5-2 km wide (Trommsdorff and Connolly 1996). Estimates of unroofing depth provided by
97 hornblende geobarometry (Davidson et al. 1996) range from ca 20 km in the Bergell main body, to
98 ca 26 km in its western tail, consistent with K-Ar biotite ages that are systematically younger than the
99 Bergell intrusion age (Villa and von Blanckenburg 1991). A smaller younger pluton, the Novate

100 granite, was intruded on the western side of the Bergell main body at 27–24 Ma (Liati et al. 2000, Ji
101 et al. 2019) (Fig. 2a).

102 Progressive erosion of these magmatic rocks together with their country rocks provided detritus
103 to the Oligocene–Miocene gravity flow deposits of the Gonfolite Group that are exposed in the
104 proximal southern foreland basin of the Alps (Wagner et al. 1979; Giger and Hurford 1989; Malusà
105 et al. 2011) (Figs. 2a, 3a) and to the more distal foredeep units now accreted in the Northern
106 Apennines (Malusà et al. 2016). The linkage between the source and the sink, long recognized by
107 compelling lithological and geochronological evidence (Wagner et al. 1979; Giger and Hurford
108 1989), is confirmed by (reverse) mineral-age stratigraphy (Malusà and Fitzgerald 2019b) and by Hf
109 isotopic composition of magmatic detrital zircon grains (Ji et al. 2019; Lu et al. 2019) (Fig. 2b).
110 Widespread volcanic detritus at the base of these stratigraphic successions (Fig. 3a) indicates that
111 volcanic eruptive centers were present atop the Bergell magmatic complex (Malusà et al. 2011;
112 Anfinson et al. 2016). Volcanic detritus was initially funnelled into submarine canyons, possibly
113 corresponding to morphologic depressions now occupied by pre-alpine lakes (Garzanti and Malusà
114 2008) and bypassed the South Alpine units triggering southward-directed gravity flows. The first
115 significant detrital pulse in the Gonfolite basin is dated biostratigraphically at ~25 Ma (Gelati et al.
116 1988) and appears to mark the onset of rapid unroofing of the Bergell area. This main erosional pulse
117 was delayed by ~5 Ma relative to the main magmatic pulse, which was associated with negligible
118 erosion and starved sedimentation in the final sink (Garzanti and Malusà 2008) (Fig. 3a). Oligocene-
119 Miocene erosion was less prominent in the South Alpine units compared to the Axial Alps, as attested
120 by ZFT ages ranging from 223 to 49 Ma, indicative of minor Cenozoic exhumation (Bertotti et al.
121 1999) (Fig. 2b).

122 **2.2. Mineral-age stratigraphy**

123 Published apatite and zircon fission-track, biotite K-Ar, and zircon U-Pb ages in cobbles in the
124 Gonfolite Group derived from the Bergell and Novate plutons and from associated country rocks are
125 summarized in Fig. 3b. These thermochronometric ages define a complex but fully predictable

126 mineral-age stratigraphy, which allows definition of three distinct mineral-age units (A to C in [Fig.](#)
127 [3](#)) characterized by specific combinations of stationary and moving age peaks ([Malusà and Fitzgerald](#)
128 [2020](#)).

129 In unit A, cobbles derived from the Bergell and Novate plutons (blue solid dots) yield syn-intrusion
130 apatite fission-track (AFT) ages that record the cooling history of the magma, whereas country-rock
131 cobbles (blue open dots) yield older AFT ages that record the pre-intrusion history of the country rock.
132 AFT ages in units B and C are the same for plutonic and country-rock cobbles and define a moving age
133 peak that gets increasingly younger upsection ([Fig. 3b](#)). These AFT ages, either marked with solid or
134 open blue dots, are systematically younger than the intrusion age of the Bergell and Novate plutons and
135 record the erosional exhumation of the plutons and surrounding country rocks.

136 ZFT analysis in units A and B yield syn-intrusive ZFT ages in cobbles derived from the Bergell and
137 Novate plutons (purple solid dots), and pre-intrusion ZFT ages in cobbles derived from the country
138 rocks (purple open dots). The first moving age peak defined by ZFT ages, recording the erosional
139 exhumation of the plutons and surrounding country rocks, only appears in mineral age unit C, as
140 denoted by the young (28-24 Ma) ZFT ages in country-rock cobbles (purple open dots in [Fig. 3b](#)).

141 Some authors have interpreted the thermochronometric ages in the Gonfolite Group within a
142 simplistic thermochronological framework by considering only the youngest age peak (e.g., [Bernoulli](#)
143 [et al. 1993](#); [Carrapa, 2009](#)). This led to suggest superfast early Oligocene erosion of the Bergell pluton
144 at a rate exceeding 6 mm/a ([Giger and Hurford, 1989](#); [Carrapa and Di Giulio, 2001](#)), which raised the
145 paradox of superfast erosion without detrital counterparts in the adjacent foreland basins ([Garzanti](#)
146 [and Malusà 2008](#); [Malusà et al. 2011](#)). Such interpretation is demonstrably incorrect, not only because
147 it clashes against compelling stratigraphic evidence (see accumulation rates in [Fig. 3a](#)), but also
148 because it fails to explain a significant part of the detrital thermochronology dataset, i.e., all the data
149 points located to the right of the vertical grey bars in [Fig. 3b](#), representing pre-intrusion mineral ages
150 in country-rock cobbles. More details on these topics and on the mineral-age stratigraphy on the

151 Gonfolite Group can be found in [Malusà et al. \(2011\)](#), [Fitzgerald et al. \(2019\)](#), and [Malusà and](#)
152 [Fitzgerald \(2019a, 2020\)](#).

153 3. Methods

154 For our study, four sandstone samples (S1 to S4) were collected for detrital ZUPb ([Malusà et al.](#)
155 [2016](#)) and ZHe analyses (this work) from the lowermost part of the Gonfolite Group, corresponding
156 to the mineral age unit A and lower part of mineral age unit B ([Fig. 3a](#)). These stratigraphic levels
157 were fed by progressive erosion of the uppermost levels of the Bergell volcanic-plutonic complex
158 and surrounding country rocks ([Giger and Hurford 1989](#); [Malusà et al. 2011](#)) and are characterized
159 by a progressive decrease in volcanic detritus and a progressive increase in plutonic detritus moving
160 up section ([Fig. 3a](#)). AFT and ZFT ages on magmatic and country rock cobbles in these stratigraphic
161 levels are independently known ([Fig. 3b](#)). Because the temperature range corresponding to the partial
162 retention zone of the ZHe system (~180-140°C; [Wolfe and Stockli 2010](#)) is in between the
163 temperature ranges of the partial annealing zones of the ZFT (~240-180°C) and AFT (~115-60°C)
164 systems (e.g., [Gleadow and Fitzgerald 1987](#)), one would expect that the analyzed zircon grains should
165 yield either ZHe ages constraining the age of magmatism or ZHe ages constraining the pre-intrusion
166 history of the country rock, but not the post-intrusive erosional exhumation history. An additional
167 sample (S5) consisting of a single cobble of country rock was collected from the mineral age unit A
168 to evaluate the intra-sample dispersion of single-grain ZHe ages.

169 All mineral separations and isotopic analyses were carried out in the UTChron Facility in the
170 Department of Geological Sciences at the University of Texas at Austin. Samples were crushed and
171 ground and detrital zircon grains were separated using standard heavy mineral and magnetic
172 separation techniques. For ZUPb LA-ICP-MS analysis, all detrital zircon grains were mounted
173 without polishing on one-inch round epoxy pucks with double sided tape, which made it possible to
174 perform subsequent ZHe analysis on the very same grains. All grains were depth-profile ZUPb dated
175 using a Photon Machines Analyte G2 ATLex 300si ArF 193 nm Excimer Laser, equipped with a

176 Helix two-volume ablation cell, and a Thermo Fisher Element2 single collector, magnetic-sector ICP-
177 MS. The reference material GJ1 (Jackson et al. 2004) was used as a primary reference and Plešovice
178 (Sláma et al. 2008) was used as a secondary reference to monitor data quality. $^{206}\text{Pb}/^{238}\text{U}$ ages are
179 reported for ages younger than 1000 Ma and $^{207}\text{Pb}/^{206}\text{Pb}$ ages are reported for ages older than 1000
180 Ma. For further details on the ZUPb analytical procedures see Malusà et al. (2016), where ZUPb ages
181 for samples S1 to S4 were originally presented.

182 U-Pb dated zircon grains with ablation pits were selected for ZHe analysis following the criteria
183 outlined in Farley (2002) and Hart et al. (2017). We exclusively chose grains for double-dating with
184 pre-Alpine ZUPb ages not derived from the Bergell complex or other Periadriatic magmatic rocks
185 (shown in Fig. 2b). We also avoided rounded grains that may have experienced removal of the grain
186 rim by abrasion during sediment transport with consequences for data interpretation, either due to
187 overcorrection for α -ejection that may lead to ZHe ages that are too old (Reiners 2005), or due to
188 unwanted comparison between ZHe ages recording magmatic crystallization and ZUPb ages from
189 inherited xenocrystic cores, which may lead to misinterpretation of magmatic ages in terms of
190 exhumation (Malusà and Garzanti 2019).

191 Selected grains were morphometrically characterized and packed into a Pt packet for in-vacuo
192 laser heating (~1300°C for 10 min) and complete degassing. Cryogenically purified and gettered He
193 was spiked with a ^3He tracer and analysis by quadrupole mass spectrometer. Degassed grains were
194 removed from the Pt packets and dissolved using a two-step HF-HNO₃ and HCl pressure vessel
195 digestion procedures. U, Th, and Sm concentrations were determined by isotope dilution using a
196 Thermo Fisher Element2 single collector, magnetic sector ICP-MS. Following Reiners (2005), Fish
197 Canyon Tuff zircons were run with unknown grains to monitor data quality. A standard error of 8%
198 was applied to all measurements. Individual analyses were excluded if the grain was partially broken
199 during unpacking from platinum packets or if there was evidence of incomplete dissolution. More
200 details on the analytical procedures for ZHe analysis are described in Wolfe and Stockli (2010).

201 4. Results

202 All ZUPb ages measured in each sample by LA-ICP-MS depth profiling and the corresponding
203 kernel density estimates are shown in Fig. 4a-e, at the bottom of each frame. The scatter plots
204 summarize the ZUPb and ZHe ages in double-dated grains not derived from Periadriatic magmatic
205 rocks (see Supplementary Table S1 for details). No grains plot on the ZUPb = ZHe line.

206 The polymodal ZUPb age distributions of samples S1 and S2, collected from mineral-age unit
207 A, are dominated by ZUPb ages pre-dating Periadriatic magmatism. Sample S1 (Fig. 4a) is dominated
208 by Caledonian and Precambrian ages, and a minor Variscan-Permian peak and a very small
209 Periadriatic peak at 32-37 Ma. Grains selected for double dating were characterized by ZUPb rim
210 ages between 282 and 457 Ma. The corresponding ZHe ages range from 29.2 ± 2.3 Ma to 278.9 ± 22.3
211 Ma.

212 Sample S2 (Fig. 4b) is dominated by Caledonian ZUPb ages, with abundant Precambrian and
213 Variscan-Permian ages, and a more prominent Periadriatic peak at 30-38 Ma than in sample S1.
214 Grains selected for double dating displayed ZUPb ages between 287 and 461 Ma with corresponding
215 ZHe ages ranging from 28.8 ± 2.3 Ma to 238.8 ± 19.1 Ma.

216 In contrast, the polymodal ZUPb age distributions of samples S3 and S4, collected from the
217 lower part of mineral-age unit B, are dominated by Periadriatic ZUPb ages, with only minor Variscan-
218 Permian, Caledonian and Precambrian age peaks. In sample S3 (Fig. 4c), Periadriatic ZUPb ages
219 exceed 60% of the dataset and range in age from 27 to 35 Ma. However, grains selected for double
220 dating were characterized by ZUPb rim ages between 272 and 296 Ma. The corresponding ZHe ages
221 ranged from 26.0 ± 2.1 Ma to 32.3 ± 2.6 Ma. In sample S4 (Fig. 4d), Periadriatic ZUPb ages exceed
222 70% of the dataset and range from 29 to 34 Ma. Grains selected for double dating yielded ZUPb ages
223 between 274 and 465 Ma. The corresponding ZHe ages ranged from 24.0 ± 1.9 Ma to 129.6 ± 10.4 Ma.

224 The country rock cobble collected from mineral-age unit A (sample S5, Fig. 4e) yielded a single
225 unimodal ZUPb age peak with a Caledonian age. Crystals selected for double dating yielded ZUPb

226 ages between 427 and 460 Ma. ZHe ages range from 108.8 ± 8.7 Ma to 189.4 ± 15.1 Ma, corresponding
227 to a central age of 146.8 ± 8.7 Ma.

228 ZHe ages vs. effective Uranium concentrations (e[U]) are summarized in the diagram of Fig. 4f.
229 Notably, many double-dated zircon grains yielded ZHe ages overlapping Bergell and Novate
230 magmatism, irrespective of their effective Uranium concentration ranging from ~100 to >1300 ppm
231 (dark grey dots in Fig. 4f).

232 5. Interpretation

233 According to the long-established mineral-age stratigraphy of the Gonfolite Group (Fig. 3b),
234 zircon grains collected from mineral-age unit A and lower part of unit B should give: (i) ZHe ages
235 overlapping the Bergell and Novate intrusion age, if zircon were derived from erosion of Bergell-
236 Novate magmatic rocks; or (ii) ZHe ages older than the Bergell and Novate intrusions, if zircon were
237 derived the country rocks that were not thermally overprinted by the intrusion. As all selected double-
238 dated zircon grains from samples S1 to S4 gave ZUPb ages between 272 and 465 Ma, they were
239 derived from erosion of the country rock. However, only a portion of these zircon grains yielded ZHe
240 ages older than the Bergell and Novate intrusions (open purple dots in Fig. 3b), whereas a substantial
241 portion of the ZHe ages yielded ages that overlap the Bergell and Novate magmatism (yellow solid
242 dots in Fig. 3b). This observation provides compelling evidence for derivation of some of the double-
243 dated zircon grains from the Bergell-Novate thermal contact aureole. Hence, these youngest ZHe ages
244 provide no direct constraints on the exhumation rate of the country rock exposed in the source area
245 for the sediment, but only record country-rock cooling in the contact aureole after magma
246 emplacement. ZHe ages in a contact aureole are expected to become progressively older, due to partial
247 resetting, moving away from the intrusion (Calk and Naeser 1973; Malusà and Fitzgerald 2019a),
248 which may explain the occurrence of a few slightly older ZHe ages of 37-39 Ma in samples S1, S2
249 and S4.

250 Insights into exhumation rates are potentially provided by the oldest ZHe ages of the dataset,
251 ranging from 62 to 279 Ma and largely fitting the distribution of single grain-ages in the analyzed
252 country rock cobble, which yielded a central age of ~147 Ma (sample S5). Because detrital
253 thermochronometric ages within a stratigraphic successions, unless reset by burial, must be equal to
254 or older than the cooling ages now observed in bedrock within the potential source areas (Malusà and
255 Fitzgerald 2020), these oldest ZHe ages support provenance from the core of the central Alps or from
256 South Alpine rocks close to the Insubric Fault, yielding a ZFT age ~49 Ma. Most of the South Alpine
257 units, instead, yielded ZFT ages from 135-177 Ma to 223 Ma in the present-day exposure level (Fig.
258 2a) and can be safely excluded as a potential source.

259 The pie charts in Fig. 3c summarize the ratio of country-rock derived zircon grains from outside
260 the Bergell and Novate contact aureole vs those derived from within the contact aureole, which yield
261 ZHe ages overlapping the Bergell and Novate intrusion ages. We observe that the percentage of ZHe
262 ages reflecting country-rock cooling in the contact aureole (in yellow in Fig. 3c) progressively
263 increases up section in the Gonfolite stratigraphic succession. This is expected because sedimentary
264 successions record the mineral-age structure of eroded bedrock in reverse order, and contact aureoles
265 are best developed at deeper structural levels surrounding large plutons rather than adjacent to
266 subvolcanic feeder dikes near the Earth's surface. Note that the percentage of syn-intrusive ZHe ages
267 recorded by country-rock derived zircon grains is an underestimate, as the partially-reset 37-39 Ma
268 ZHe ages were not included in the budget.

269 **6. Revised criteria for the interpretation of double-dated mineral grains**

270 *6.1 Expected thermochronologic age combinations*

271 Our findings delineate a tripartite scenario, in terms of age combinations expected for high-
272 temperature (e.g., ZUPb) and low-temperature (e.g., ZHe) geo/thermochronometric systems, when
273 zircon grains eroded from a shallow-level volcanic-plutonic complex and associated country rocks
274 are correctly analyzed via double-dating including ZUPb analysis that targets the zircon rim. These

275 three cases are illustrated in the upper row of Fig. 5 (Cases 1 to 3), which shows an unpolished depth-
276 profiled zircon grain similarly to the approach applied in this work: *Case (1)* - Zircon grains derived
277 from shallow-level magmatic rocks; *Case (2)* - Zircon grains derived from the contact aureole; and
278 *Case (3)* - Zircon grains derived from country rocks not thermally affected by the intrusion. The lower
279 row of Fig. 5 (Cases 4 to 6) shows instead, for comparison, a polished zircon grain with an ablation
280 pit on the center of the grain, similarly to the approach followed in several previous works (e.g., Shen
281 et al. 2012; Jourdan et al. 2013, 2018; Stevens 2013; Bootes et al. 2019). Notably, if the ablated
282 central part of the grain includes a xenocrystic core (e.g., Corfu et al. 2003), this will provide a core
283 $ZUPb_{(C)}$ age that can be remarkably older than the rim $ZUPb_{(R)}$ age of the depth-profiled zircon rim.

284 Zircon grains derived from shallow-level magmatic rocks (Case 1 in Fig. 5) are expected to yield
285 ZHe ages that record ultra-rapid cooling following at the time of intrusion (T_i) and that are
286 indistinguishable within error from the rim $ZUPb_{(R)}$ age of the depth-profiled zircon rims. Zircon
287 grains derived from the contact aureole (Case 2 in Fig. 5) are instead expected to yield ZHe ages = T_i
288 that reflect country-rock cooling immediately after intrusion, and that are younger than the pre-
289 intrusion rim $ZUPb_{(R)}$ ages of the zircon. These ZHe ages are expected to become progressively older
290 moving away from the intrusion. Finally, zircon grains derived from country rocks not affected by
291 the intrusion (Case 3 in Fig. 5) should yield ZHe ages $> T_i$ that are generally younger than the rim
292 $ZUPb_{(R)}$ age of the corresponding zircon rim.

293 Note that the ZHe system provides constraints to the age of magmatism both for Case 1 and Case
294 2. However, only for Case 1 do zircon grains show $ZUPb_{(R)} = ZHe$ or a fingerprint that can be
295 exploited for the identification of magmatic ages. Zircon grains derived from the contact aureole
296 show instead $ZUPb_{(R)} > ZHe$, which implies that those ZHe ages cannot be identified as magmatic
297 ages by a classic approach to double dating. Because only part of the grains yielding magmatic ZHe
298 ages can be identified by double dating (i.e., $ZUPb_{(R)} = ZHe$), the assumption that all the remaining
299 grains preserve an exhumation signal invariably leads to interpretations that are prone to be incorrect.

300 **6.2 Zircon core vs zircon rim U-Pb ages**

301 Another important point underlined in [Fig. 5](#), cases 4 to 6, is that core $ZUPb_{(C)}$ ages are always
302 $> ZHe$ ages in all the three cases considered. Therefore, a double-dating approach targeting zircon
303 cores is not suitable for detecting magmatic ages in detrital zircon grains, unless the occurrence of
304 xenocrystic cores can be safely excluded. Hence, it is critical to determine the youngest magmatic
305 age zone of a zircon for double dating. So far, only few detrital thermochronometric studies have
306 targeted the grain rim for ZUPb analysis in the context of double dating. For example, [Rahl et al.](#)
307 [\(2003\)](#) performed LA-ICP-MS analysis in a single pit $\sim 30 \mu m$ in diameter and $\sim 20 \mu m$ deep on the
308 exterior of unmodified grains mounted on tape. [Najman et al. \(2010\)](#) performed ZUPb analysis on
309 grain external surfaces with ablation crater depths of $\sim 4\text{-}10 \mu m$. [Pujols and Stockli \(2021\)](#) mounted
310 unpolished zircons on acrylic disks for LA-ICP-MS depth profiling to recover the ZUPb age of the
311 youngest growth zone from each grain. Many other works, for example [Stevens et al. \(2013\)](#) and
312 [Jourdan et al. \(2013, 2018\)](#) explicitly targeted the core of zircon grains for their ZUPb analyses.
313 [Bootes et al. \(2019\)](#) preablated the grains with a $40\text{-}\mu m$ diameter spot followed by a $20\text{-}\mu m$ diameter
314 spot that penetrated to a depth of $\sim 12 \mu m$ for data collection at zircon cores, whereas [Lu et al. \(2020\)](#)
315 performed LA-ICP-MS ZUPb dating through multiple $30 \mu m$ spots located within the same area
316 where ZFT were counted, also including the core of the zircon grains. The double-dating approach
317 that was applied in this second category of studies likely precluded a correct identification of
318 magmatic ages in those grains with a xenocrystic core, despite their potential derivation from shallow-
319 level magmatic rocks. Additional complications may arise due to removal of grain rims by abrasion
320 during sediment transport. In this case, zircon grains derived from erosion of magmatic rocks may
321 only preserve the ZUPb age of an inherited core even in the most external parts of the grain ([Malusà](#)
322 [and Garzanti 2019](#)). As a result, magmatic ZHe ages are prone to be incorrectly interpreted in terms
323 of exhumation, because $ZUPb_{(C)} > ZHe$. Crucial for a correct interpretation is therefore an
324 independent knowledge of the age T_i of the main magmatic events in a study region. This information,
325 although sometimes not available *a priori*, can be easily retrieved in detrital thermochronology
326 studies by identification of the $ZUPb_{(R)} = ZHe$ fingerprint in double-dated zircon grains.

327 *6.3 Implications for lag-time analysis*

328 In the previous section we have underlined the importance of a double-dating approach targeting
329 zircon rims for a correct identification of magmatic ages. For the sake of simplicity, in this section
330 we assume that double-dated grains from previous studies contain no xenocrystic cores, to dismiss
331 any potential problems due to an incorrect location of the ZUPb ablation spot. However, even under
332 such favorable hypothetical circumstance, our results from the Bergell-Gonfolite system indicate that
333 the assumption that all double-dated grains with a ZUPb > ZHe fingerprint preserve an exhumation
334 signal is invariably misleading. Our findings are particularly relevant in detrital thermochronology
335 studies that emphasize the importance of the youngest thermochronologic age peaks for lag-time
336 analysis. Because ZHe = T_i for Case 2 and ZHe > T_i for Case 3 (Fig. 5), magmatic ZHe ages derived
337 from the contact aureole (Case 2) are systematically younger than any potential exhumation ZHe age
338 in nearby country rocks unaffected by the intrusion (Case 3). Therefore, zircon grains from a contact
339 aureole always form the youngest ZHe age peak in the polymodal grain-age distribution derived from
340 erosion of a single volcanic-plutonic source. Even if magmatic ages recognized by their ZUPb_(R) =
341 ZHe fingerprint (1 in Fig. 1) are systematically removed from the data set, the interpretation of the
342 youngest ZHe (or ZFT) age peak in terms of exhumation remains prone to misinterpretations.

343 As a rule, zircon grains likely derived from country rock (ZUPb_(R) > ZHe) but sharing the same
344 ZHe age with zircon grains that are undoubtedly magmatic according to their ZUPb=ZHe fingerprint
345 (3 in Fig. 1), should be excluded from any interpretation in terms of exhumation using the lag-time
346 approach. If there is a suspicion that part of these ZHe ages may derive from a different source and
347 may therefore represent exhumation ages, this must be demonstrated in a stratigraphic sequence
348 where the contribution of ZHe magmatic ages (ZUPb=ZHe) is not present. Note that zircon grains
349 derived from country rock and from much younger magmatic rocks may, and often do share the same
350 ZHe exhumation age in specific intervals of a stratigraphic succession. However, exhumation ages
351 are always younger than the intrusion age T_i of mineral grains derived from the same source (Malusà

352 and Fitzgerald 2020). Therefore, these situations are readily identifiable because no grains lie on the
353 $ZUPb = ZHe$ (or $ZUPb = ZFT$) line.

354 7. Application to previous studies

355 The concepts described in section 6 can be applied to published high-quality double-dating
356 datasets from the literature. For example, Figure 6a shows ZUPb and ZFT data from zircon grains of
357 the Zhaguo Member, Tethyan Himalaya (Najman et al. 2010). ZUPb analysis was performed on grain
358 external surfaces. Most grains have similar ZUPb and ZFT ages (marked red in Fig. 6a), which were
359 interpreted as formation ages from an igneous source. The remaining grains have Precambrian ZUPb
360 ages and were interpreted, based on their ZFT age, as being exhumed from depth during the Mesozoic
361 (Najman et al. 2010). However, most of these grains (marked yellow in Fig. 6a) have ZFT ages
362 systematically overlapping the ZFT ages of grains lying on the $ZUPb=ZFT$ line, which are clearly
363 magmatic. Therefore, these ZFT ages provide no direct indication on exhumation. Instead, these ZFT
364 ages may either record country-rock cooling in a contact aureole, or crystallization of shallow-level
365 magmatic rocks as recorded by zircon grains that include xenocrystic cores improperly analyzed for
366 ZUPb dating. Only a single grain of the dataset (marked green in Fig. 6a) can possibly provide
367 information on exhumation, albeit loosely constrained due to the large error bar of this ZFT age (Fig.
368 6a).

369 A similar situation is observed in Fig. 6b, showing a data set based on the analysis of modern
370 sands of the Ordos Basin in north-central China (Stevens et al. 2013). The authors have specifically
371 targeted zircon cores for their ZUPb analyses. They found a majority of grains showing Permo-
372 Triassic ZFT ages independent on ZUPb ages. A number of grains showing overlapping ZUPb and
373 ZFT age at ~250 Ma was interpreted as the indication of relatively shallow emplacement and rapid
374 exhumation at the source. However, these ages (marked red in Fig. 6b) simply record crystallization
375 of shallow-level magmatic rocks and cannot be used to deduce an exhumation rate. The same applies
376 for the many grains with a similar ZFT age but a much older ZUPb age (marked yellow in Fig. 6b)

377 which provide no useful constraints on exhumation. The greater percentage of zircon grains marked
378 in yellow in Fig. 6b compared to Fig. 6a is likely the effect of a biased approach in ZUPb analysis
379 targeting zircon cores rather than zircon rims, which may have precluded a correct identification of
380 magmatic ages in many zircon grains with older xenocrystic cores. Only four grains on the entire
381 dataset (marked green in Fig. 6b) can therefore potentially provide information on exhumation.

382 The occurrence of a majority of grains with an old ZUPb age and a young ZFT age that overlaps
383 magmatic ZFT ages of grains yielding ZUPb=ZFT is common to several other studies (e.g., Shen et
384 al. 2012; Jourdan et al. 2013, 2019). Jourdan et al. (2013) applied a double-dating approach including
385 ZFT analysis and ZUPb dating of zircon cores in sedimentary rocks on either side of the Western
386 Alps (Fig. 7). In the western Alpine foreland basin, they identified three zircon groups: (i) a first
387 group with overlapping Paleogene ZUPb and ZFT ages representing ~10% of the dataset and
388 interpreted as volcanically derived Paleogene zircon grains; (ii) a second group encompassing ~66%
389 of the data set and including zircons with Paleogene ZFT ages and much older, mainly Variscan ZUPb
390 ages; and (iii) a third group characterized by a wide range of Cretaceous–Jurassic ZFT ages and much
391 older (Variscan or Panafrican) ZUPb ages. Jourdan et al. (2013) excluded from the dataset the ZFT
392 ages of the first group zircons to obtain what they considered a pure exhumation signal. Based on
393 ZFT ages ~30–31 Ma in the second group zircons from Oligocene sediments (marked by a blue star
394 in Fig. 7a), they proposed a short-lived rapid exhumation event affecting the Western Alps during the
395 early Oligocene, triggered by indentation of the Adriatic upper mantle beneath the eclogitic units of
396 the Internal Zone (dark blue in Fig. 7c) and consequent surface uplift and rapid erosion of the Western
397 Alps at rates exceeding 1.5–2 km/Ma. However, zircon grains with ZUPb > ZFT, but sharing the
398 same ZFT age with zircon grains of the first group that are undoubtedly magmatic because ZUPb =
399 ZFT, should be excluded from any interpretation in terms of exhumation. It may be argued that part
400 of these zircon grains may derive from a different source compared to the zircon grains of the first
401 group, and that their ZFT ages may potentially represent exhumation ages. However, as introduced
402 in Sect. 6.3, this hypothesis must be tested in a stratigraphic succession where any potential

403 contributions of magmatic ZFT ages can be safely excluded. The Monferrato sedimentary succession,
404 exposed to the east of the Western Alps (Fig. 7b, c), provides a favorable opportunity to check whether
405 detrital ZFT data supports the hypothesis of an Oligocene exhumation signal or not. These sediments
406 were demonstrably fed by detritus shed from the Alpine Internal Zone (Elter et al. 1966; Polino et al.
407 1991). They contain ZUPb ages that are Jurassic or older, but no Paleogene ZUPb age, pointing to a
408 negligible contribution of Paleogene magmatism to the detrital thermochronologic record. Because
409 the youngest ZFT age peak in Oligocene sediments of the Monferrato spans from 39 to 78 Ma, but
410 no peak ~30 Ma is observed (question mark in Fig. 7b), we conclude that detrital ZFT data from either
411 side of the orogen provide no evidence of early Oligocene fast erosional exhumation in the Western
412 Alps, unlike suggested by Jourdan et al. (2013). In the western Alpine foreland basin, ZFT ages of
413 second group zircons thus record country-rock cooling in a contact aureole or crystallization of
414 shallow-level magmatic rocks as recorded by ZUPb dating of old xenocrystic cores. Potential
415 candidate sources for these zircon grains are magmatic complexes located to the south-west (e.g.,
416 Provence, Sardinia) or to the north-east (e.g., Biella) of the sampling location (Fig. 7c). These
417 potential sources may have provided zircon grains to the western Alpine foreland basin, but
418 apparently no zircon grains to the Monferrato.

419 If a complementary stratigraphic succession without magmatic ZFT ages is not available, further
420 clues for a correct interpretation of double-dated mineral grains can be provided by the analysis of
421 thermochronologic age trends through a stratigraphic succession (Fig. 7a) following the criteria
422 illustrated in Malusà and Fitzgerald (2020). Thermochronologic ages that are set during episodes of
423 magmatic crystallization define stationary age peaks that remain fixed up section (see in Fig. 7a the
424 points that lies on the 30 Ma dotted line). These stationary age peaks can be detected in the detrital
425 thermochronologic record starting from strata deposited synchronously with magmatism.
426 Thermochronologic ages that are set during bedrock erosion define instead moving age peaks that
427 gets progressively younger up section. Notably, the first appearance of a moving age peak that records
428 erosional exhumation only occurs with a considerable time delay in the sedimentary succession fed

429 by erosion, depending on the closure temperature of the thermochronologic system under
430 consideration and the erosion rate. In fact, the whole rock pile with a thermochronologic fingerprint
431 acquired before the onset of erosion must first be completely removed (Malusà and Fitzgerald 2020).
432 For example, ZFT ages recording the onset of fast erosion at rates ~2 km/Ma starting at ~30 Ma would
433 be only expected in sedimentary strata with depositional age of ~ 27-26 Ma or younger. Since the
434 ZFT ages ~30-31 Ma (blue star in Fig. 7a) in the western Alpine foreland basin were detected in
435 layers with a depositional age of ~30 Ma, we can conclude that these ages provide information on
436 magmatism, not exhumation, consistent with the information previously provided by the analysis of
437 the Monferrato complementary stratigraphic sequence (Fig. 7b).

438 8. Conclusions

439 ZUPb and ZHe double dating of selected detrital zircon grains from the sedimentary succession
440 of the Gonfolite Group allows us to revise the criteria that had been previously applied in detrital
441 thermochronometric studies in terms of identification and discrimination of magmatic and
442 exhumation ages. In a detrital thermochronometric dataset, we found that only part of the grains
443 yielding magmatic ZHe (or ZFT) ages can be identified by their $ZUPb_{(R)} = ZHe$ (or ZFT) fingerprint.
444 A relevant percentage of syn-intrusive ZHe (or ZFT) cooling ages that record country-rock cooling
445 in a contact aureole remain undetected because these ages are younger than the corresponding
446 $ZUPb_{(R)}$ age in the same zircon grains. Because only part of the grains yielding magmatic ZHe or
447 ZFT ages can be identified by a classic double-dating approach, the assumption that all the remaining
448 grains may provide information on exhumation is invariably misleading. Interpretation is even more
449 critical in those studies targeting zircon cores for ZUPb dating, because such approach is not suitable
450 for systematically and reliably detecting magmatic ages in detrital zircon grains. Our findings are
451 particularly relevant for detrital thermochronometric studies that emphasize the importance of the
452 youngest thermochronologic age peaks for lag-time analysis, as zircon grains from a contact aureole
453 always form the youngest thermochronologic age peak in polymodal grain-age distributions derived

454 from erosion of the uppermost levels of a single volcanic-plutonic source. This is particularly
455 pertinent for basin deposits that are sourced from orogenic hinterlands characterized by voluminous
456 magmatism, such as magmatic arcs in convergent tectonics settings.

457 Based on our analysis, we illustrate improved criteria for the interpretation of double-dated
458 mineral grains in detrital thermochronology studies. Their application to high-quality datasets of
459 double-dated grains from the literature suggest that many previous geologic interpretations based on
460 a classic double-dating approach should be proficiently reconsidered. Our results underline not only
461 the potential of a double-dating approach that includes ZUPb analysis of unpolished depth-profiled
462 zircon grains, but also demonstrate the importance of a proper analysis of thermochronologic age
463 trends through a stratigraphic succession for a correct geologic interpretation of detrital
464 thermochronology data.

465 **CRedit authorship contribution statement**

466 *Marco G. Malusà*: Conceptualization, Formal Analysis, Visualization, Writing – original draft,
467 Writing – review & editing. *Owen Anfinson*: Conceptualization, Investigation, Formal Analysis,
468 Writing – review & editing, Funding acquisition. *Daniel F. Stockli*: Methodology, Resources, Writing
469 – review & editing, Funding acquisition.

470 **Declaration of competing interest**

471 The authors declare that they have no known competing financial interests or personal relationships
472 that could have appeared to influence the work reported in this paper.

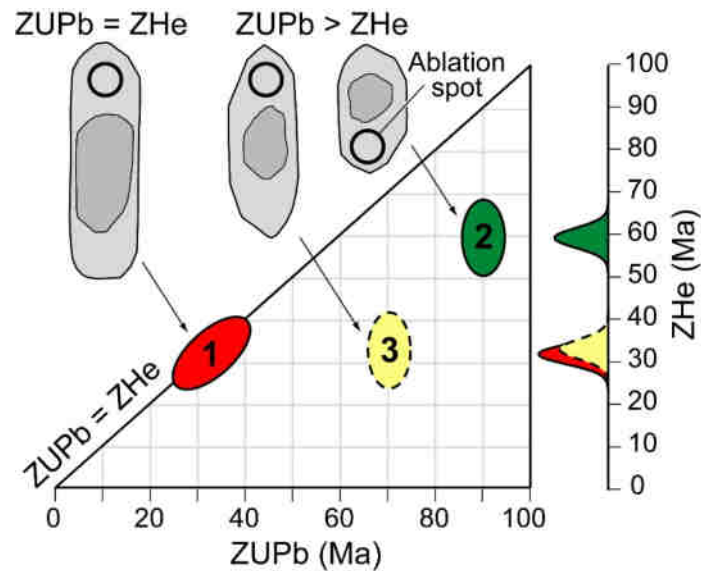
473 **Acknowledgments**

474 We thank Paul G. Fitzgerald and Igor M. Villa for insightful discussions on the interpretation of
475 detrital thermochronology datasets, Lisa Stockli, Spencer Semen and Andrew Smye for significant
476 contributions to the development and implementation of analytical procedures, and the UTChron
477 Laboratory, the University of Texas at Austin for providing financial support for this project. The

478 clarity of the manuscript was significantly improved thanks to the positive comments provided by
479 two anonymous reviewers.

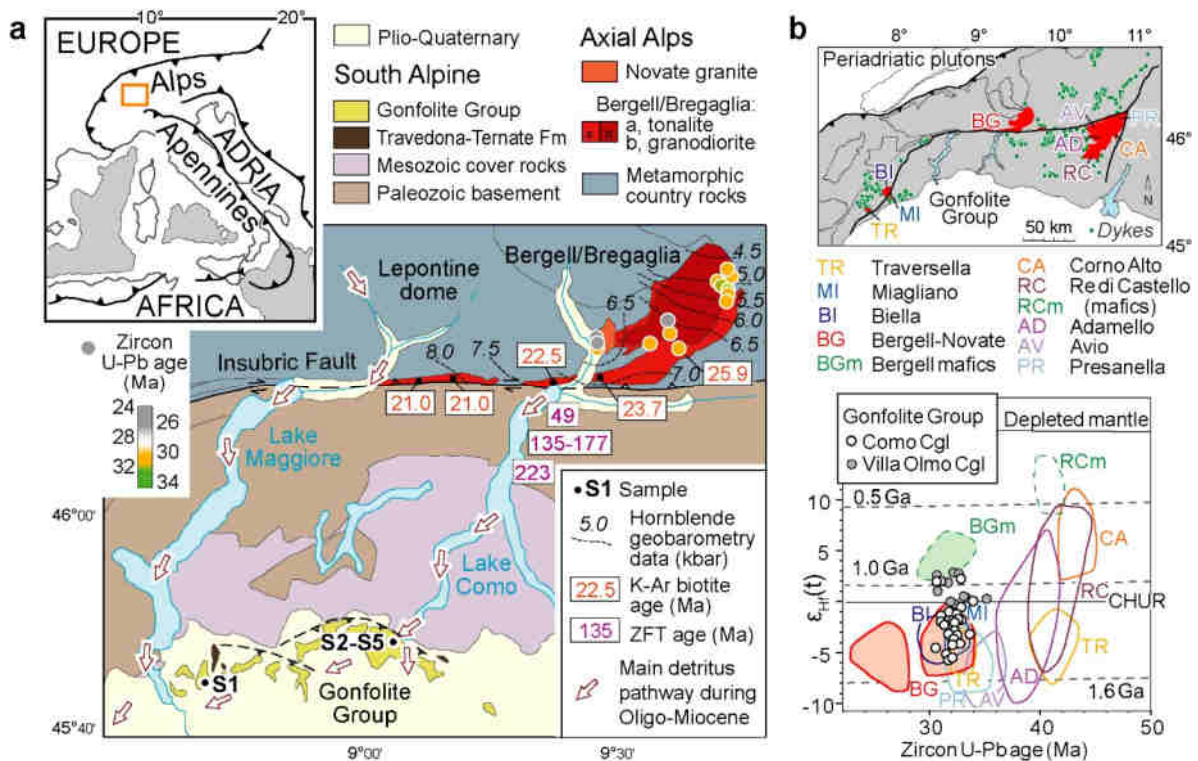
480 **Appendix A. Supplementary material**

481 **Supplementary Table S1:** Sample locations, reduced (U-Th)/He data, and U-Pb data of double-
482 dated zircon grains.



484

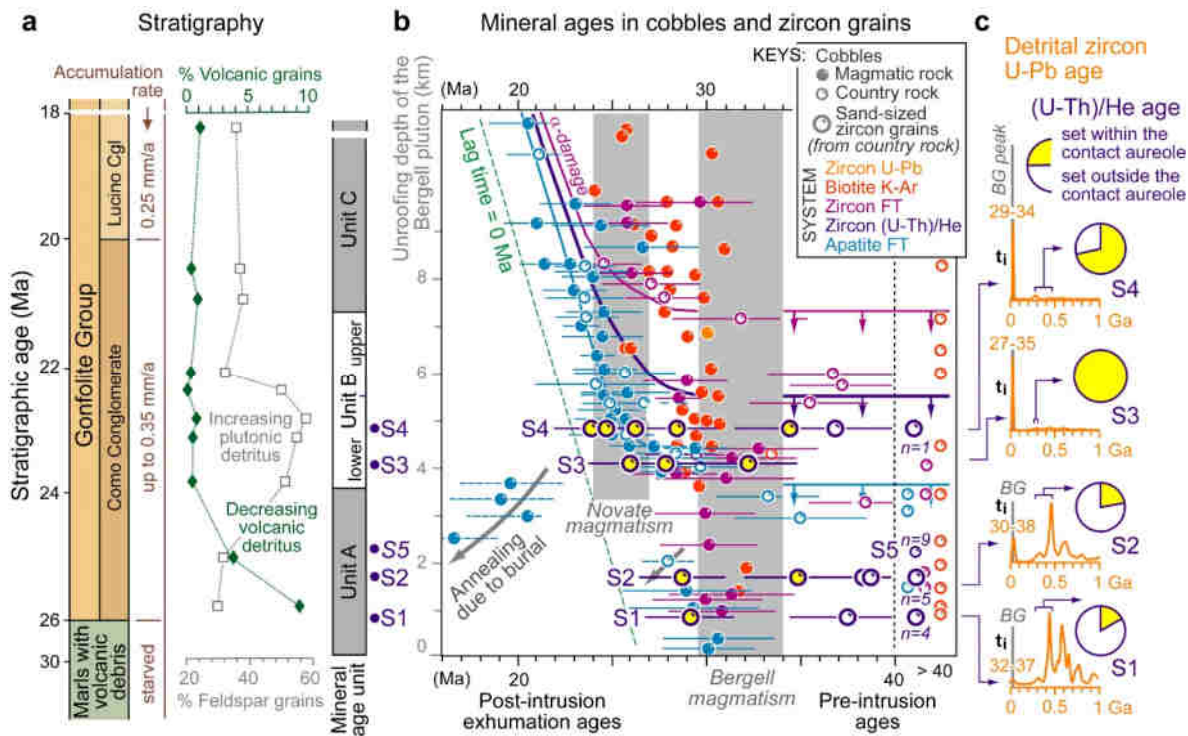
485 **Figure 1: Rationale of the double-dating approach for the identification of magmatic ages in**
 486 **detrital zircon grains.** Paired high-temperature and low-temperature geo/thermochronologic
 487 analyses, such as zircon U-Pb (ZUPb) and (U-Th)/He (ZHe) or fission-tracks, are applied to the same
 488 detrital grains (Carter and Bristow 2003; Reiners et al. 2005). Zircon grains yielding magmatic ZHe
 489 ages are readily identified by their ZUPb=ZHe fingerprint (1), provided that older xenocrystic cores
 490 are avoided during ZUPb analysis (Malusà and Fitzgerald 2020). The remaining grains, yielding low-
 491 temperature thermochronometric ages younger than the corresponding ZUPb age (2, 3) are often used
 492 to infer the exhumation history of the source rocks (e.g., Najman et al. 2010; Stevens et al. 2013;
 493 Jourdan et al. 2013, 2018; Bootes et al. 2019; Lu et al. 2020). Grains marked (3), unlike grains marked
 494 (2), share the same ZHe age with zircon grains marked (1) that are undoubtedly magmatic according
 495 to their ZUPb=ZHe fingerprint.



497

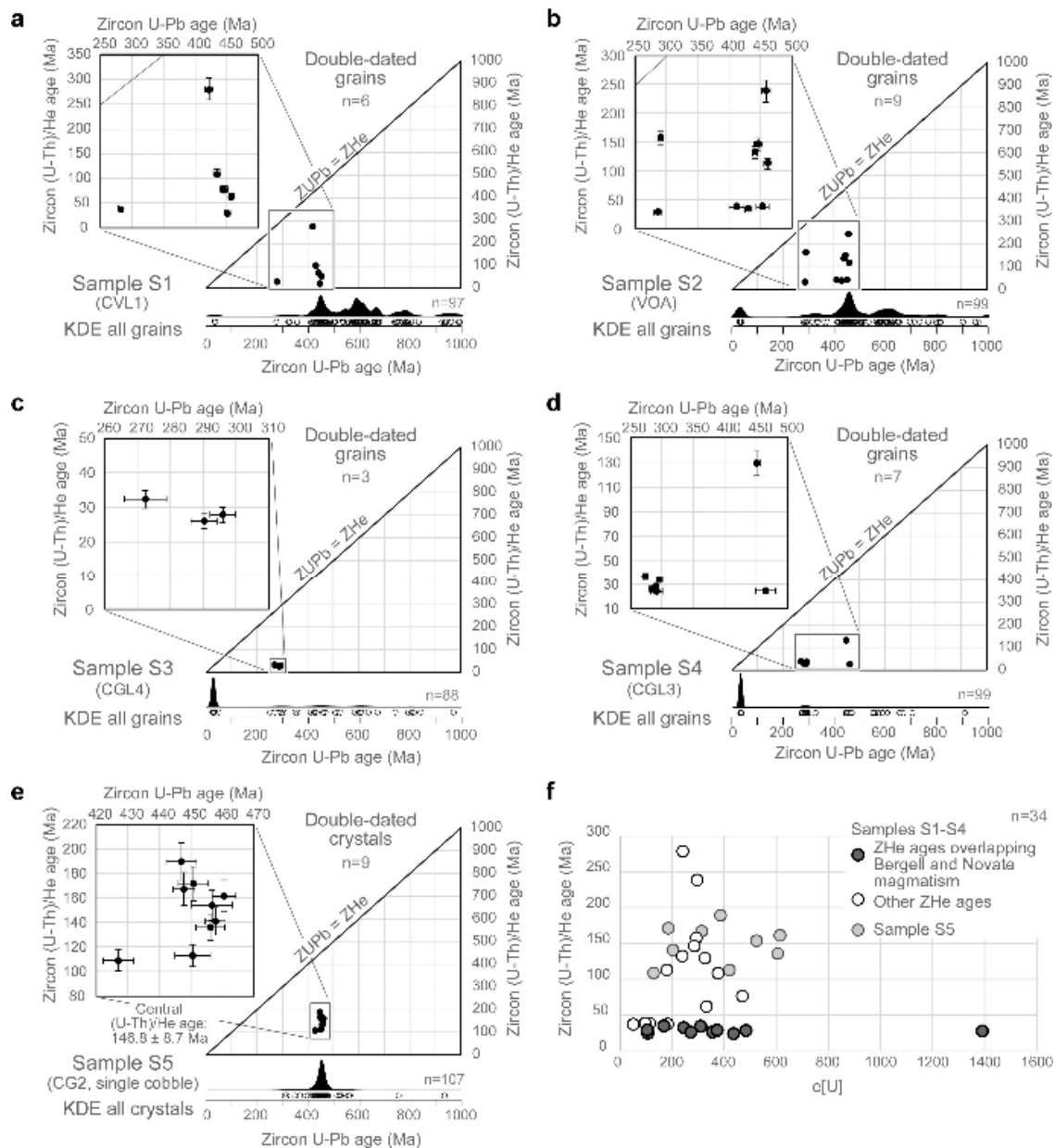
498 **Figure 2: Tectonic framework.** **a** Geologic sketch map of the Bergell-Gonfolite source-to-sink
 499 system (see location in the inset). Lakes Como and Maggiore occupy Oligocene-Miocene
 500 paleovalleys funnelling detritus towards the Gonfolite basin (after [Malusà et al. 2011](#)). Relevant
 501 bedrock zircon U-Pb ages ([Ji et al. 2019](#)), hornblende geobarometry data ([Davidson et al. 1996](#)),
 502 biotite K-Ar ages ([Villa and von Blanckenburg 1991](#)), and zircon fission-track (ZFT) ages ([Bertotti](#)
 503 [et al. 1999](#)) are also shown. S1 to S5 indicate samples of the Gonfolite Group analyzed in this work
 504 (the coordinates for each sample are indicated in the supplementary material, their biostratigraphic
 505 ages are reported in [Malusà et al. 2016](#)). **b**: U-Pb ages and Hf isotopic compositions of magmatic
 506 zircon grains of the Gonfolite Group compared to the reference fields of the potential Periadriatic
 507 sources shown in the map (after [Malusà and Fitzgerald 2020](#), based on data from [Ji et al. 2019](#) and
 508 [Lu et al. 2019](#)).

Figure 3



510

511 **Figure 3: Mineral-age stratigraphic framework.** **a:** Simplified stratigraphic column, accumulation
 512 rate, modal composition, and mineral-age units of the Gonfolite Group (from Malusà et al. 2011). **b:**
 513 Mineral ages in magmatic cobbles (small solid dots) and country rock cobbles (small open dots)
 514 provided by apatite and zircon fission-track, biotite K-Ar and zircon U-Pb dating (from Malusà et al.
 515 2011 and references therein; see color coding on the top-right). The vertical grey bars indicate the
 516 age of Bergell and Novate magmatism (Ji et al. 2019). Continuous lines in color indicate predicted
 517 patterns of pre-intrusion and exhumation ages (Malusà et al. 2011; Malusà and Fitzgerald 2020). (U-
 518 Th)/He ages of double-dated zircon grains from samples S1 to S5 (this work) are also shown (larger
 519 dots, in violet). The yellow fill indicates zircon (U-Th)/He ages overlapping with Bergell and Novate
 520 magmatism. n is the number of double-dated zircon grains yielding (U-Th)/He ages older than 40 Ma
 521 in each sample. **c:** Zircon U-Pb kernel density estimates of samples S1 to S4. Numbers in orange
 522 indicate the age range of the youngest U-Pb age peaks (from Malusà et al. 2016). The pie charts
 523 summarize the ratio of country-rock derived zircon grains showing (U-Th)/He ages set within the
 524 Bergell and Novate contact aureole vs those derived from outside the contact aureole (this work;
 525 arrows mark the corresponding U-Pb age ranges). BG = Bergell-Novate.

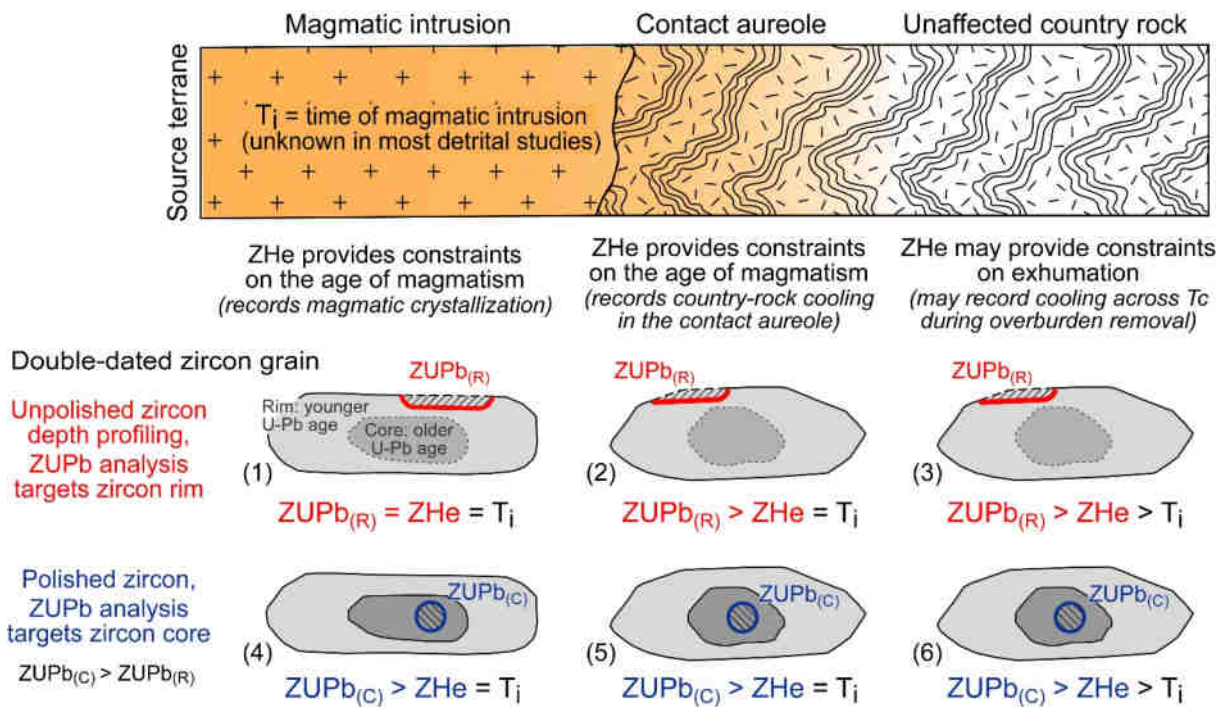


527

528 **Figure 4: Double-dating results.** a-d: Zircon U-Pb kernel density estimates (KDE) for detrital
 529 samples S1 to S4 (from Malusà et al. 2016, see stratigraphic locations in Fig. 3a). Open dots are single
 530 U-Pb ages measured by LA-ICP-MS depth profiling of unpolished zircon grains (n= number of dated
 531 grains). Scatter plots show double-dated zircon grains (solid dots with 2σ error bars) that were
 532 selected following the criteria outlined in Farley (2002) among those zircon grains not derived from
 533 Periadriatic magmatic rocks, as indicated by their U-Pb age. Note that no grains plot on the $ZUPb =$

534 ZHe line, which would ensure that (U-Th)/He ages of these double-dated zircon grains constrain
535 exhumation, not magmatic crystallization (e.g., [Jourdan et al. 2013](#); [Bootes et al. 2019](#); [Lu et al.](#)
536 [2020](#)). **e:** Double-dated zircon crystals from a single country-rock cobble (sample S5). **f:** Zircon (U-
537 Th)/He age (ZHe) vs. effective Uranium concentration (e[U]) in double-dated zircon grains from
538 samples S1 to S5. ZHe ages overlapping Bergell and Novate magmatism are indicated in dark grey
539 (these ZHe ages characterize the zircon grains derived from erosion of country rock affected by the
540 Bergell and Novate contact aureole).

541



543

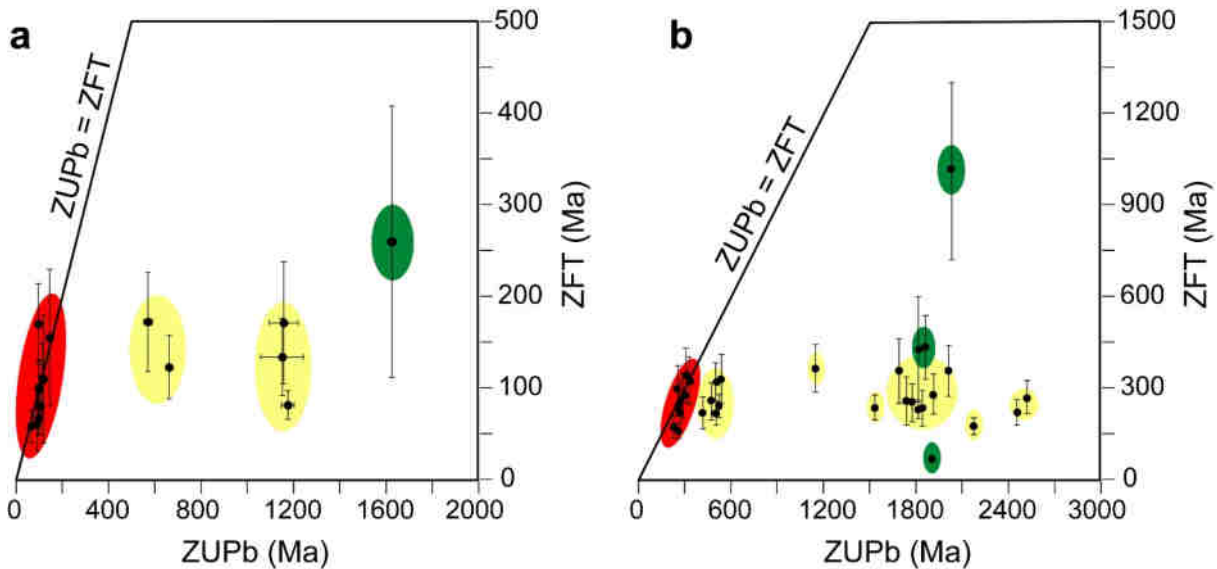
544 **Figure 5: Potential misidentification of exhumation ages by double dating.** The cartoon shows
 545 the ages expected for high-temperature (e.g. ZUPb) and low-temperature (e.g., ZHe)
 546 thermochronologic systems when zircon grains eroded from a shallow-level volcanic-plutonic
 547 complex and its country rocks are correctly analyzed by a double-dating approach with ZUPb analysis
 548 that targets the zircon rim (Cases 1 to 3, upper row in red). Results expected when ZUPb analysis
 549 targets an older xenocrystic core is shown for comparison (Cases 4 to 6, lower row in blue). *Case (1)*
 550 - Zircon grains derived from shallow-level magmatic rocks: they yield ZHe ages that record magmatic
 551 crystallization at time T_i and that are indistinguishable within error from the $ZUPb_{(R)}$ ages yielded by
 552 depth profiling of the grain rim. *Case (2)* - Zircon grains derived from the contact aureole: they yield
 553 ZHe ages = T_i that reflect country-rock cooling immediately after intrusion and that are younger than
 554 the pre-intrusion $ZUPb_{(R)}$ ages of the grain rim. *Case (3)* - Zircon grains derived from country rocks
 555 not affected by the intrusion: they yield ZHe ages $> T_i$ that are younger than the $ZUPb_{(R)}$ ages of the
 556 grain rim. Note that the ZHe system provides constraints to the age of magmatism both for case (1)
 557 and case (2). However, only for case (1) do zircon grains show $ZUPb_{(R)} = ZHe$. Because only part of
 558 the grains yielding magmatic ZHe ages can be identified by double dating (i.e., $ZUPb_{(R)} = ZHe$), the
 559 assumption that all the remaining grains provide constraints on exhumation is prone to lead to

560 incorrect interpretations. *Cases (4) to (6)* - When ZUPb analysis targets a xenocrystic core, the
561 ZUPb_(C) age is invariably older than the corresponding ZHe age.

562

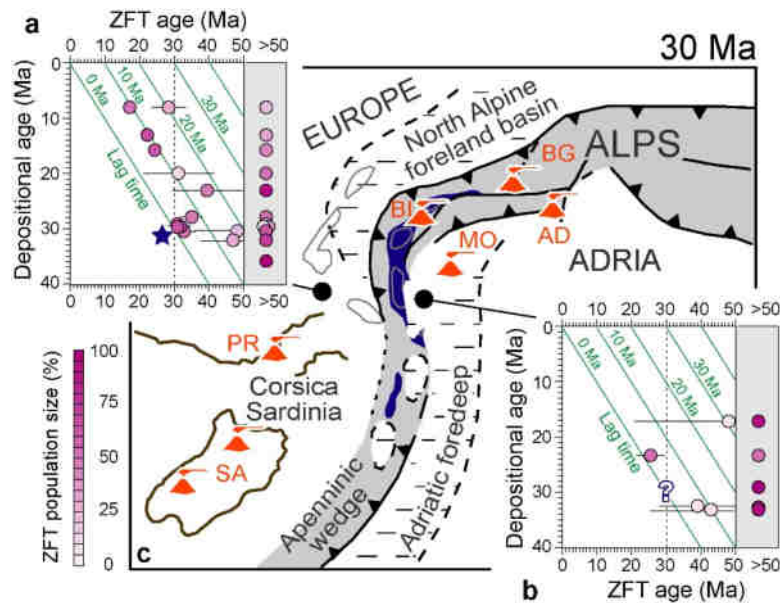
563

Figure 6



564

565 **Figure 6: Application to previous studies. a:** Double-dated zircon grains from the Zhaguo Member,
566 Tethyan Himalaya (Najman et al. 2010). **b:** Double-dated zircon grains from modern sands of the Mu
567 Us desert, Ordos Basin, north central China (Stevens et al. 2013). Both zircon U-Pb (ZUPb) and
568 zircon fission-track (ZFT) ages were quoted at 2 sigma errors. ZUPb analysis targeted the grain rim
569 in (a) and the grain core in (b). Keys: Red = ZFT ages that record magmatic crystallization of shallow-
570 level magmatic rocks; Yellow = ZFT ages that may record country-rock cooling in a contact aureole
571 or magmatic crystallization (due to ZUPb dating of old xenocrystic cores); Green = ZFT ages that
572 may provide constraints on exhumation (see Malusà and Fitzgerald 2020 for further details). Both red
573 and yellow marked grains should be excluded from exhumation rate calculations based on lag-time
574 analysis (see text for explanation). Note the increasing proportion of double-dated zircon grains
575 marked yellow when ZUPb analysis targets the zircon core (b).



577

578 **Figure 7: Insights from thermochronologic age trends through a stratigraphic succession. a-b:**
 579 Detrital ZFT data from the western Alpine foreland basin (a) (Bernet et al., 2009; Jourdan et al., 2013)
 580 and the Monferrato (b) (Jourdan et al., 2013). Different color intensities in the lag-time diagrams
 581 indicate the relative percentages of each grain-age population (Malusà and Fitzgerald 2020). Grains
 582 older than 50 Ma are shown as a single population for the sake of simplicity. The vertical dashed line
 583 at 30 Ma marks the end of the Alpine magmatic climax. The dark blue star in (a) indicates prominent
 584 populations of double-dated zircon grains interpreted by Jourdan et al. (2013) as evidence of short-
 585 lived, fast erosional exhumation of the Western Alps at ~30 Ma. However, the question mark in (b)
 586 shows that similar ZFT ages are not found in basins located to the east of the Western Alps, which
 587 were demonstrably fed by detritus shed from the Alpine Internal Zone. **c:** Palinspastic reconstruction
 588 of the Alps-Apennines system at 30 Ma showing the exhumed eclogitic units of the Internal Zone
 589 (dark blue), active magmatic complexes (in orange), and the locations of the samples shown in (a)
 590 and (b) (solid black dots). Acronyms: AD, Adamello; BI, Biella and Traversella; BG, Bergell; MO,
 591 Mortara; PR, Provence; SA, Sardinia (Anfinson et al. 2016).

592 **References**

- 593 1. Anfinson, O. A., Malusà, M. G., Ottria, G., Dafov, L. N., & Stockli, D. F. (2016). Tracking
594 coarse-grained gravity flows by LASS-ICP-MS depth-profiling of detrital zircon (Aveto
595 Formation, Adriatic foredeep, Italy). *Marine and Petroleum Geology*, 77, 1163-1176.
- 596 2. Bernet, M., van der Beek, P., Pik, R., Huyghe, P., Mugnier, J. L., Labrin, E., & Szulc, A.
597 (2006). Miocene to recent exhumation of the central Himalaya determined from combined
598 detrital zircon fission-track and U/Pb analysis of Siwalik sediments, western Nepal. *Basin
599 Research*, 18(4), 393-412.
- 600 3. Bernet, M., Brandon, M., Garver, J., Balestieri, M. L., Ventura, B., & Zattin, M. (2009).
601 Exhuming the Alps through time: Clues from detrital zircon fission-track thermochronology.
602 *Basin Research*, 21(6), 781-798.
- 603 4. Bernoulli, D., Giger, M., Müller, D.W., Ziegler, U.R.F. (1993). Sr-isotope-stratigraphy of the
604 Gonfolite Lombarda Group ("South-Alpine Molasse", northern Italy) and radiometric
605 constraints for its age of deposition. *Eclogae Geol. Helv.* 86, 751–767.
- 606 5. Bertotti, G., Seward, D., Wijbrans, J., Ter Voorde, M., & Hurford, A. J. (1999). Crustal
607 thermal regime prior to, during, and after rifting: a geochronological and modeling study of
608 the Mesozoic South Alpine rifted margin. *Tectonics*, 18(2), 185-200.
- 609 6. Bootes, N., Enkelmann, E., & Lease, R. (2019). Late Miocene to Pleistocene source to sink
610 record of exhumation and sediment routing in the Gulf of Alaska from detrital zircon fission-
611 track and U-Pb double dating. *Tectonics*, 38(8), 2703-2726.
- 612 7. Calk, L. C., & Naeser, C. W. (1973). The thermal effect of a basalt intrusion on fission tracks
613 in quartz monzonite. *The Journal of Geology*, 81(2), 189-198.
- 614 8. Carrapa, B. (2009). Tracing exhumation and orogenic wedge dynamics in the European Alps
615 with detrital thermochronology. *Geology*, 37(12), 1127-1130.

- 616 9. Carrapa, B., & Di Giulio, A. (2001). The sedimentary record of the exhumation of a granitic
617 intrusion into a collisional setting: the lower Gonfolite Group, Southern Alps, Italy.
618 *Sedimentary Geology*, 139(3-4), 217-228.
- 619 10. Carter, A., & Bristow, C. S. (2003). Linking hinterland evolution and continental basin
620 sedimentation by using detrital zircon thermochronology: a study of the Khorat Plateau Basin,
621 eastern Thailand. *Basin Research*, 15(2), 271-285.
- 622 11. Carter, A., & Moss, S. J. (1999). Combined detrital-zircon fission-track and U-Pb dating: A
623 new approach to understanding hinterland evolution. *Geology*, 27(3), 235-238.
- 624 12. Corfu, F., Hanchar, J. M., Hoskin, P. W., & Kinny, P. (2003). Atlas of zircon textures.
625 *Reviews in mineralogy and geochemistry*, 53(1), 469-500.
- 626 13. Davidson, C., Rosenberg, C., & Schmid, S. M. (1996). Synmagmatic folding of the base of
627 the Bergell pluton, Central Alps. *Tectonophysics*, 265(3-4), 213-238.
- 628 14. Elter, G., Elter, P., Sturani, C., & Weidman, M. (1966). Sur la prolongation du domaine ligure
629 de l'Apennin dans le Monferrat et les Alpes et sur l'origine de la Nappe de la Simme s. l. des
630 Préalpes romande et chablaisiennes: *Bulletin des Laboratoires de Géologie, Minéralogie,*
631 *Géophysique et du Musée Géologique de l'Université de Lausanne*, v. 167, p. 61-72.
- 632 15. England, P., & Molnar, P. (1990). Surface uplift, uplift of rocks, and exhumation of rocks.
633 *Geology*, 18(12), 1173-1177.
- 634 16. Farley, K. A. (2002). (U-Th)/He dating: Techniques, calibrations, and applications. *Reviews*
635 *in Mineralogy and Geochemistry*, 47(1), 819-844.
- 636 17. Fitzgerald, P. G., Malusà, M. G., & Muñoz, J. A. (2019). Detrital thermochronology using
637 conglomerates and cobbles. In *Fission-Track Thermochronology and its Application to*
638 *Geology* (pp. 295-314). Springer, Cham.

- 639 18. Garver, J. I., Brandon, M. T., Roden-Tice, M., & Kamp, P. J. (1999). Exhumation history of
640 orogenic highlands determined by detrital fission-track thermochronology. *Geological*
641 *Society, London, Special Publications*, 154(1), 283-304.
- 642 19. Garzanti, E., & Malusà, M. G. (2008). The Oligocene Alps: Domal unroofing and drainage
643 development during early orogenic growth. *Earth and Planetary Science Letters*, 268(3-4),
644 487-500.
- 645 20. Gelati, R., Napolitano, A., & Valdisturlo, A. (1988). La " Gonfolite Lombarda": stratigrafia e
646 significato nell'evoluzione del margine sudalpino. *Rivista Italiana di Paleontologia e*
647 *Stratigrafia*, 94(2).
- 648 21. Giger, M., & Hurford, A.J. (1989). Tertiary intrusives of the Central Alps: their Tertiary uplift,
649 erosion, redeposition and burial in the south-Alpine foreland. *Eclogae Geol. Helv.* 82, 857–
650 866.
- 651 22. Gleadow, A. J. W., & Fitzgerald, P. G. (1987). Uplift history and structure of the
652 Transantarctic Mountains: new evidence from fission track dating of basement apatites in the
653 Dry Valleys area, southern Victoria Land. *Earth and planetary science letters*, 82(1-2), 1-14.
- 654 23. Govin, G., van der Beek, P., Najman, Y., Millar, I., Gemignani, L., Huyghe, P., ... & Wijbrans,
655 J. (2020). Early onset and late acceleration of rapid exhumation in the Namche Barwa
656 syntaxis, eastern Himalaya. *Geology*, 48(12), 1139-1143.
- 657 24. Hart, N. R., Stockli, D. F., Lavier, L. L., & Hayman, N. W. (2017). Thermal evolution of a
658 hyperextended rift basin, Mauléon Basin, western Pyrenees. *Tectonics*, 36(6), 1103-1128.
- 659 25. Jackson, S. E., Pearson, N. J., Griffin, W. L., & Belousova, E. A. (2004). The application of
660 laser ablation-inductively coupled plasma-mass spectrometry to in situ U–Pb zircon
661 geochronology. *Chemical geology*, 211(1-2), 47-69.

- 662 26. Ji, W. Q., Malusà, M. G., Tiepolo, M., Langone, A., Zhao, L., & Wu, F. Y. (2019).
663 Synchronous Periadriatic magmatism in the Western and Central Alps in the absence of slab
664 breakoff. *Terra Nova*, 31(2), 120-128.
- 665 27. Jourdan, S., Bernet, M., Tricart, P., Hardwick, E., Paquette, J. L., Guillot, S., ... & Schwartz,
666 S. (2013). Short-lived, fast erosional exhumation of the internal western Alps during the late
667 early Oligocene: Constraints from geothermochronology of pro-and retro-side foreland basin
668 sediments. *Lithosphere*, 5(2), 211-225.
- 669 28. Jourdan, S., Bernet, M., Hardwick, E., Paquette, J. L., Tricart, P., Senebier, F., & Coeur, F.
670 (2018). Geo-thermochronology of the Saint Antonin basin, south-eastern France Géo-
671 thermochronologie du bassin de Saint Antonin, sud-est de la France. *Bulletin de la Société*
672 *Géologique de France*, 189(3).
- 673 29. Lang, K. A., Glotzbach, C., Ring, U., Kamp, P. J., & Ehlers, T. A. (2020). Linking orogeny
674 and orography in the Southern Alps of New Zealand: New observations from detrital fission-
675 track thermochronology of the Waiho-1 borehole. *Earth and Planetary Science Letters*, 552,
676 116586.
- 677 30. Liati, A., Gebauer, D., & Fanning, M. (2000). U-Pb SHRIMP dating of zircon from the Novate
678 Granite (Bergell, Central Alps); evidence for Oligocene-Miocene magmatism,
679 Jurassic/Cretaceous continental rifting and opening of the Valais Trough. *Schweizerische*
680 *mineralogische und petrographische Mitteilungen*, 80(3), 305-316.
- 681 31. Lossada, A. C., Hoke, G. D., Giambiagi, L. B., Fitzgerald, P. G., Mescua, J. F., Suriano, J., &
682 Aguilar, A. (2020). Detrital Thermochronology Reveals Major Middle Miocene Exhumation
683 of the Eastern Flank of the Andes That Predates the Pampean Flat Slab (33°–33.5° S).
684 *Tectonics*, 39(4), e2019TC005764.
- 685 32. Lu, G., Di Capua, A., Winkler, W., Rahn, M., Guillong, M., von Quadt, A., & Willett, S. D.
686 (2019). Restoring the source-to-sink relationships in the Paleogene foreland basins in the

- 687 Central and Southern Alps (Switzerland, Italy, France): A detrital zircon study approach.
688 International Journal of Earth Sciences, 108(6), 1817-1834.
- 689 33. Lu, G., Fellin, M. G., Winkler, W., Rahn, M., Guillong, M., von Quadt, A., & Willett, S. D.
690 (2020). Revealing exhumation of the central Alps during the Early Oligocene by detrital
691 zircon U–Pb age and fission-track double dating in the Taveyannaz Formation. International
692 Journal of Earth Sciences, 109(7), 2425-2446.
- 693 34. Malusà, M. G., & Fitzgerald, P. G. (2019a). From cooling to exhumation: setting the reference
694 frame for the interpretation of thermochronologic data. In Fission-track thermochronology
695 and its application to geology (pp. 147-164). Springer, Cham.
- 696 35. Malusà, M. G., & Fitzgerald, P. G. (2019b). Application of thermochronology to geologic
697 problems: bedrock and detrital approaches. In Fission-Track Thermochronology and its
698 Application to Geology (pp. 191-209). Springer, Cham.
- 699 36. Malusà, M. G., & Fitzgerald, P. G. (2020). The geologic interpretation of the detrital
700 thermochronology record within a stratigraphic framework, with examples from the European
701 Alps, Taiwan and the Himalayas. Earth-Science Reviews, 201, 103074.
- 702 37. Malusà, M. G., & Garzanti, E. (2019). The sedimentology of detrital thermochronology. In
703 Fission-Track Thermochronology and its Application to Geology (pp. 123-143). Springer,
704 Cham.
- 705 38. Malusà, M. G., Villa, I. M., Vezzoli, G., & Garzanti, E. (2011). Detrital geochronology of
706 unroofing magmatic complexes and the slow erosion of Oligocene volcanoes in the Alps.
707 Earth and Planetary Science Letters, 301(1-2), 324-336.
- 708 39. Malusà, M. G., Anfinson, O. A., Dafov, L. N., & Stockli, D. F. (2016). Tracking Adria
709 indentation beneath the Alps by detrital zircon U-Pb geochronology: Implications for the
710 Oligocene–Miocene dynamics of the Adriatic microplate. Geology, 44(2), 155-158.

- 711 40. Najman, Y., Appel, E., Boudagher-Fadel, M., Bown, P., Carter, A., Garzanti, E., ... & Vezzoli,
712 G. (2010). Timing of India-Asia collision: Geological, biostratigraphic, and palaeomagnetic
713 constraints. *Journal of Geophysical Research: Solid Earth*, 115(B12).
- 714 41. Polino, R., Ruffini, R., & Ricci, B. (1991). Le molasse terziarie della collina di Torino:
715 relazioni con la cinematica alpina. *Atti Ticinensi Scienze della Terra*, 34, 85-95.
- 716 42. Pujols, E. J., & Stockli, D. F. (2021). Zircon (U-Th)/(He-Pb) double-dating constraints on the
717 interplay between thrust deformation and foreland basin architecture, Sevier foreland basin,
718 Utah. *Geosphere*, 17(6), 1890-1913.
- 719 43. Rahl, J. M., Reiners, P. W., Campbell, I. H., Nicolescu, S., & Allen, C. M. (2003). Combined
720 single-grain (U-Th)/He and U/Pb dating of detrital zircons from the Navajo Sandstone, Utah.
721 *Geology*, 31(9), 761-764.
- 722 44. Reiners, P. W. (2005). Zircon (U-Th)/He thermochronometry. *Reviews in Mineralogy and*
723 *Geochemistry*, 58(1), 151-179.
- 724 45. Reiners, P. W., Campbell, I. H., Nicolescu, S., Allen, C. M., Hourigan, J. K., Garver, J. I., ...
725 & Cowan, D. S. (2005). (U-Th)/(He-Pb) double dating of detrital zircons. *American Journal*
726 *of Science*, 305(4), 259-311.
- 727 46. Saylor, J. E., Stockli, D. F., Horton, B. K., Nie, J., & Mora, A. (2012). Discriminating rapid
728 exhumation from syndepositional volcanism using detrital zircon double dating: Implications
729 for the tectonic history of the Eastern Cordillera, Colombia. *Bulletin*, 124(5-6), 762-779.
- 730 47. Shen, C. B., Donelick, R. A., O'Sullivan, P. B., Jonckheere, R., Yang, Z., She, Z. B., ... & Ge,
731 X. (2012). Provenance and hinterland exhumation from LA-ICP-MS zircon U-Pb and fission-
732 track double dating of Cretaceous sediments in the Jiangnan Basin, Yangtze block, central
733 China. *Sedimentary Geology*, 281, 194-207.

- 734 48. Sláma, J., Košler, J., Condon, D. J., Crowley, J. L., Gerdes, A., Hanchar, J. M., ... &
735 Whitehouse, M. J. (2008). Plešovice zircon—a new natural reference material for U–Pb and
736 Hf isotopic microanalysis. *Chemical Geology*, 249(1-2), 1-35.
- 737 49. Stevens, T., Carter, A., Watson, T. P., Vermeesch, P., Andò, S., Bird, A. F., ... & Sevastjanova,
738 I. (2013). Genetic linkage between the Yellow River, the Mu Us desert and the Chinese loess
739 plateau. *Quaternary Science Reviews*, 78, 355-368.
- 740 50. Stockli, D. F., & Najman, Y. M. (2020). Earth's dynamic past revealed by detrital
741 thermochronometry. *Elements: An International Magazine of Mineralogy, Geochemistry, and*
742 *Petrology*, 16(5), 311-317.
- 743 51. Trommsdorff, V., & Connolly, J. A. (1996). The ultramafic contact aureole about the
744 Bregaglia (Bergell) tonalite: isograds and a thermal model. *Schweizerische Mineralogische*
745 *und Petrographische Mitteilungen*, 76, 537-547.
- 746 52. Villa, I. M., & von Blanckenburg, F. (1991). A hornblende ^{40}Ar - ^{39}Ar age traverse of the
747 Bregaglia tonalite (southeast Central Alps). *Schweizerische Mineralogische und*
748 *Petrographische Mitteilungen*, 71, 73-87.
- 749 53. von Blackenburg, F. (1992). Combined high-precision chronometry and geochemical tracing
750 using accessory minerals: applied to the Central-Alpine Bergell intrusion (central Europe).
751 *Chemical Geology*, 100(1-2), 19-40.
- 752 54. Wagner, G. A., Miller, D. S., & Jäger, E. (1979). Fission track ages on apatite of Bergell rocks
753 from central Alps and Bergell boulders in Oligocene sediments. *Earth and Planetary Science*
754 *Letters*, 45(2), 355-360.
- 755 55. Wolfe, M. R., & Stockli, D. F. (2010). Zircon (U–Th)/He thermochronometry in the KTB drill
756 hole, Germany, and its implications for bulk He diffusion kinetics in zircon. *Earth and*
757 *Planetary Science Letters*, 295(1-2), 69-82.